Solid State Sciences 143 (2023) 107286

Contents lists available at ScienceDirect

Solid State Sciences

journal homepage: www.elsevier.com/locate/ssscie

The role of cluster microstructure on the exchange coupling interaction between magnetically hard and soft phases

S. Ferrari [a,b,*], R. Martínez García [a], F. Morales [a,c], M. Pagnola [a,b]

[a] CONICET - Universidad de Buenos Aires, Instituto de Tecnologías y Ciencias de la Ingeniería "Hilario Fernández Long" (INTECIN), Av. Paseo Colón 850, (C1063ACV), Buenos Aires, Argentina

[b] Universidad de Buenos Aires, Facultad de Ingeniería, Departamento de Física, Laboratorio de Sólidos Amorfos, Av. Paseo Colón 850, (C1063ACV), Buenos Aires, Argentina

[c] Departamento Física de la Materia Condensada, Centro Atómico Constituyentes, Comisión Nacional de Energía Atómica, Av. General Paz 1499, (B1650), Villa Maipú, Pcia. de Buenos Aires, Argentina

ARTICLE INFO

Keywords:
Nanostructured magnetic composite
$BaFe_{12}O_{19}/NiFe_2O_4$
Structural and magnetic characterization

ABSTRACT

Nanocomposites of Al-doped Barium Ferrites mixed with Nickel Ferrite were synthesized and characterized using various techniques. We investigated the role of cluster microstructure on the exchange coupling interaction between magnetically hard and soft phases in nanostructured composites consisting of Al-doped barium ferrites mixed with nickel ferrite. The magnetic response of the composites showed an "S-shaped" curve, but there were weak or no signs of magnetic exchange coupling, even though the nanoparticles of the two phases had a ratio within the range where this interaction would be possible. The presence of the mentioned clusters can explain the latter phenomenon. We quantified microstructural parameters and analyzed their correlation with magnetic behavior, focusing on two specific composites: one with minimal magnetic interaction (80% $BaFe_{12}O_{19}$ and 20% $NiFe_2O_4$) and another with no interaction (80% $BaFe_{10.5}Al_{1.5}O_{19}$ and 20% $NiFe_2O_4$). In the mentioned samples a distribution of sizes of the clusters of $NiFe_2O_4$ were obtained by image analysis of the EDAX nickel mapping picture. Also Henkel plots were used to determine the quantity and distribution of dipolar magnetic interaction and exchange coupling magnetic interaction between the phases. The composites exhibited a disordered microstructure with clusters of $NiFe_2O_4$ dispersed in the $BaFe_{12}O_{19}$ matrix. Our results indicate that the size of the clusters is an important factor in determining the strength of the exchange coupling interaction. Our findings have implications for designing and optimizing magnetic materials with enhanced exchange coupling interaction.

1. Introduction

The current diversity of devices that use permanent magnets is increasing due to the need for them in performing control tasks and as in-situ sensors. Additionally, the bearer equipment containing the permanent magnets needs to be less bulky and more efficient, requiring magnets with a higher energy product $(BH)_{max}$ to optimize their operation and maximize the processes involving these materials. Currently, rare earth magnets with Sm–Co and Nd-Fe-B [1,2] offer the best (BH) max, making them essential for manufacturing everything from smartphones to wind turbines. Consequently, the production of these critical resources has significantly increased.

To illustrate the scale of their current usage, a 1-MW wind turbine requires one ton of permanent magnets, while a "zero-emission" car relies on approximately 1 kg of neodymium for its engine and around 10 kg of other rare earths for its rechargeable batteries. These green technologies heavily depend on these resource metals to achieve a reduction in CO_2 emissions. However, meeting the soaring demand for rare earths poses significant challenges as only a few countries have direct access to them. Therefore, materials such as M-type magnetic hexaferrites present attractive magnetic properties (saturation magnetization (M_s) up to 60 emu/g [3] and coercive field (H_c) up to 7000 Oe [4]) to serve as replacements for rare-earth magnets. In particular, the M-type hexaferrite material of Barium hexaferrite (BaM), has ferrimagnetic nature and a magnetoplumbite crystal structure [5,6], possesses a host of advantageous properties. It exhibits high magnetic coercivity, chemical stability,

* Corresponding author. CONICET - Universidad de Buenos Aires, Instituto de Tecnologías y Ciencias de la Ingeniería "Hilario Fernández Long" (INTECIN), Av. Paseo Colón 850, (C1063ACV), Buenos Aires, Argentina.
E-mail address: sferrari@fi.uba.ar (S. Ferrari).

https://doi.org/10.1016/j.solidstatesciences.2023.107286
Received 13 May 2023; Received in revised form 2 August 2023; Accepted 14 August 2023
Available online 19 August 2023

high Curie temperature, electrical resistivity, and cost-effectiveness. These characteristics make it a valuable material for diverse applications such as microwave absorbers, magnetic recording media, channel filters, tuning slugs, and microwave gyromagnetic devices [5–7]. Its ability to retain magnetization even in the presence of a strong magnetic field is crucial for preventing easy reversibility. Moreover, its chemical stability and high Curie temperature enable reliable performance in harsh environments and high-temperature applications. The high electrical resistivity of barium hexaferrite renders it suitable for impeding the flow of electric current when necessary. Notably, its relatively low production cost adds to its appeal as a cost-effective choice for various applications. In summary, barium hexaferrite stands as a versatile ferrimagnetic material with a wide range of properties that make it highly valuable across multiple fields.

The study of permanent magnets and exchange bias materials has a long history. However, it is only recently that researchers have been able to create composite materials that exhibit both properties. The challenges of creating such a material are twofold: suppressing the exchange bias effect in a small region of the material, and matching the properties of the permanent magnet and exchange bias regions. Despite these challenges, there has been significant progress in the development of composite materials with both permanent magnet and exchange bias properties. These materials have the potential to revolutionize a wide range of applications.

The mentioned properties of Barium hexaferrite are currently not enough for achieving a superior higher performance magnet, necessary to replace rare earth permanent magnets, with alternative materials making them an attractive proposition for the magnet industry. Again recalling wich we have stated about composites: one potential solution is the development of magnetic compounds that exhibit an increased energy product $(BH)_{max}$ by combining a magnetically hard phase with a soft phase together. In such compounds, the hard magnetic phase contributes a large coercive field, while the soft magnetic phase contributes a high saturation magnetization. If an exchange coupling is achieved between the two phases, the compound's energy product can be enhanced [8]. Consequently, scientific research investigating the exchange coupling interactions between soft and hard magnetic phases holds vital importance. From the wide range of soft magnetic materials, we choose nickel ferrite since with its distinctive qualities, has been extensively researched and stands out among various ferrites. It possesses remarkable physical properties, including stability, good mechanical hardness, and reasonable saturation magnetization. The inverse spinel crystal structure of nickel ferrite contributes to its unique magnetic properties, encompassing paramagnetic, superparamagnetic, and ferrimagnetic characteristics. These properties are influenced by the composition and microstructure, which, in turn, are sensitive to the preparation methods employed. Notably, nickel ferrites exhibit high electrical resistivity and low magnetic coercivity, making them highly versatile. This has led to their application in transformer cores, microwave devices, magnetic storage devices in electronics and telecommunication, targeted drug delivery agents in medicine, and their utilization as agents for lithium-ion batteries and nano catalysis in the energy industry [9,10].

In $BaFe_{12}O_{19}/NiFe_2O_4$ composites, like the ones we explore in our article, the interface between particles or grains in these composites plays a crucial role, as for noted for example in ref [11] where it stand the importance of this phenomena in this composites for the magnetic properties. In general the interface phenomenon plays a significant role in determining the properties of composite materials, influencing their electrical, magnetic, and mechanical characteristics. Extensive studies on interface phenomena in composites have been conducted, emphasizing their relevance in enhancing specific properties. In literature there are some good examples that shed light of the importance of interface phenomena like in ref. [12] where it explores the role of interface charge in the giant electrocaloric effect observed in thin films, that leads to a substantial polarization change and enhances coupling between ferroelectric domains; in Ref. [13] it is studied the $BiFeO_3/SrTiO_3$ heterostructure system where the interface between the two materials can play a key role in the emergence of multiferroicity, as it can provide a new energy landscape that can stabilize multiferroicity; in ref.[14] alludes to a co-precipitated Ni/Mn shell-coated nanocubes system where the interface between the Ni/Mn shell can play an important part in the emergence of multiferroicity, as it can provide a new energy landscape that can stabilize multiferroicity; lastly, in ref. [15] a magnetic field coupling fractional step lattice Boltzmann (FSLB) model is proposed to simulate the complex interfacial behaviors in magnetic multiphase flows, illustrating that the interface between different phases in a magnetic multiphase flow has a crucial function in the complex interfacial behavior, as it can mediate the interactions between the phases and affect the flow dynamics.

In this study, we focus, instead of interface phenomena, on investigating the role of microstructure (particulary in the formation of clusters of one of the phases) in the strength of exchange-coupling magnetic interactions between barium hexaferrite (as the hard magnetic phase) and nickel ferrite (as the soft magnetic phase) within magnetic compounds. We find that the exchange coupling interaction is stronger when the clusters are smaller and more dispersed, and when they are aligned in a parallel fashion. These findings have important implications for the development of new and improved composites with enhanced magnetic properties.

To achieve these findings, we have used the image proccessing program ImageJ [16] for analizing the $NiFe_2O_4$ clusters sizes present in the EDAX generated Nickel element mapping picture, and we also have used magnetic Henkel plots [17] as a tools to assess the degree of magnetic coupling between the phases. Specifically, we examine two composite mixtures: one with maximum magnetic moment density (composite of $BaFe_{12}O_{19} + NiFe_2O_4$ in 80/20 wt% proportions) and the other with minimum magnetic moment density (composite of $BaFe_{10.5}Al_{1.5}O_{19}$ + 20% $NiFe_2O_4$ in 80/20 wt% proportions). We quantify certain microstructural parameters in these composites, specifically focusing on clusters of $NiFe_2O_4$ dispersed within the matrix volume of barium hexaferrite. In the first mixture, magnetic coupling is minimal, while in the second mixture, such interaction is nonexistent. Finally, by comparing histograms of cluster sizes and Henkel curves, we infer a relationship between microstructure and magnetic exchange interactions.

2. Experimental

2.1. Synthesis of doped aluminium hexagonal ferrite

Powders of Aluminium doped barium ferrite nanoparticles with formula $BaFe_{12-x}Al_xO_{19}$ ($x = 0, 0.5, 1.0, 1.5$) were obtained by the citrate Sol-Gel method. The sol-gel method was chosen because it is a versatile technique that can be used to synthesize ferrites with a variety of properties and is advantageous over traditional methods such as the solid-state reaction method because it can produce ferrites with fine particles of nanosize, which have improved magnetic properties. The sol-gel method is also relatively easy and inexpensive, and it can be carried out at relatively low temperatures. The fine particle size of ferrites produced by the sol-gel method results in improved magnetic properties because the smaller particles have a higher surface area, which allows for more effective exchange interactions between the magnetic ions. As a result, sol-gel ferrites have higher saturation magnetization and coercivity than ferrites produced by other traditional methods [18].

The method of synthesis is well described in our recent article [19]. The only difference in the method, concerning the cited article, is that in the case of Al-doped samples ($x \neq 0$), we added aluminium III nitrate, in the needed stoichiometry amount for the aimed formula, as an additional precursor salt to incorporate the Al element in the final ferrite. All samples had a final heat treatment of ramp with a heating rate of

5 °C/min until they reached 1000 °C, temperature which was maintained for 5 h, until that the oven was turned off and we have waited that all cooled down to room temperature. We are assuring that all the samples the same final heat treatment to obtain that the same value of crystallite size, which is a key factor in the final magnetic properties. In this way we can relate the changes in magnetism respect the undoped sample only directly to the factor of the content of aluminium in the crystal structure.

2.2. Synthesis of nickel ferrite

A single sample of powder cubic ferrite nanoparticles $NiFe_2O_4$ was obtained by co-precipitation mixing diluted salts of Fe and Ni in the 2:1 stoichiometry ratio, and then adding a solution of diluted NaOH as a precipitating agent. This technique is already described in various articles [20–22].

The final treatment of the sample is at 1000 C°, with identical procedure to the one applied to Al-doped barium ferrites. The selection of temperature is based on the fact that, we already have shown in our previous article [7], in which we have proved that the best magnetic properties in the $BaFe_{12}O_{19}/NiFe_2O_4$ composite are achieved when both of components have the same order of crystallite size.

2.3. Obtaining $BaFe_{12-x}Al_xO19/NiFe_2O_4$ nanostructured magnetic composites

The composites of Al-doped barium Ferrite and composites were obtained from the mixture of 80% by weight of one of the Al-doped hexagonal ferrite nanoparticle sample, $BaFe_{12-x}AlxO_{19}$, and 20% by weight of cubic ferrite nanoparticles, $NiFe_2O_4$. Each different barium ferrite sample, with different doping content of Al, was joined with a part of the same unique sample of nickel ferrite in weight ratio explained. After that, the mixing was done by mechanical milling in a ball mill with a frequency of 10 Hz for 1 h. Finally, a heat treatment at 1000 °C for 5 h was applied to the composites to relax tensions created during the milling process. Table 1 shows the composition, heat treatment, and nomenclature of all samples.

2.4. Samples characterization

X-ray diffraction (XRD) data was obtained with a Rigaku D-Max diffractometer with Cu-K_α (λ = 0,15418 nm) radiation. In order to determine quantitative phases GSAS-II program [23] was used. Magnetic measurements of Al-doped Barium ferrites were done with a in a Vibrating Sample Magnetometer (VSM) up to 3000 kA/m where hysteresis loops (M vs. H) were obtained at room temperature. Electronic Microscope images and EDAX element mapping was performed with a Scanning Electronic Microscope.

3. Results and discussion

For a better comprehension of the properties of the materials fabricated by us, we divide the description of them in two sections, in the first section (3.1) we describe the experimental results of the Al-doped barium ferrites and the nickel ferrite (precursors), and in the second section (3.2) we describe the results of the mixtures (composites).

Table 1
Composition and nomenclature of the precursors samples.

Nomenclature	Sample composition
BAL0	$BaFe_{12.0}Al_{0.0}O_{19}$
BAL0.5	$BaFe_{11.5}Al_{0.5}O_{19}$
BAL1.0	$BaFe_{11.0}Al_{1.0}O_{19}$
BAL1.5	$BaFe_{10.5}Al_{1.5}O_{19}$

3.1. Al-doped barium ferrites and nickel ferrite results (precursors)

We have produced two kinds of precursors, the Al-doped Barium Ferrites with formula $BaFe_{12-x}$ Al_xO_{19} made by Sol-Gel citrate method, and a single nickel ferrite powder sample made by co-precipitation. The following nomenclature is used to refer to the Al-doped Barium Ferrites.

3.1.1. X-ray diffraction results

Fig. 1 shows the XRD patterns corresponding to the Al-doped barium ferrites, while Fig. 2 shows the XRD pattern corresponding to the nickel ferrite. All the XRD patterns of the Al-doped barium ferrites presented Fig. 1 with different content of Aluminium presented the diffraction peaks of $BaFe_{12}O_{19}$ structure (S.G. $P6_3/mmc$ (194), sys. Hexagonal (ICSD # 201654 see Ref. [24]) and the presence of a small quantity (around 5%) of hematite. Meanwhile the XRD presented in Fig. 2 shows only the phase corresponding to cubic crystal structure $NiFe_2O_4$ (S.G. Fd-3m (227) sys. cubic (ICSD # 076179 see Ref. [25]). The absence of alumina or aluminium peaks in the patterns in Fig. 1 is an indirect source of confirmation that aluminium has been incorporated as a dopant in the lattice of barium ferrite, as desired. More evidence of this incorporation will be presented below.

We can see in the X-ray diffraction patterns of the Al-doped barium ferrites that there is a change in the intensity relation ratio of the principal peaks. This change in intensity ratio is caused by the modification of the overall X-ray cross section of the crystallographic planes of the hexaferrite due to the presence of Aluminum atoms within them. At the same time, if we observe Table 2, where we report the cell constants obtained by Rietveld refinement, there is a contraction of the cell. The decrease of cell constants (see Fig. 3) is an expected result, due to the fact that the ionic radius of Al^{+3} is 53 p.m. which is smaller than the ionic radius of Fe^{+3} which is 65 p.m. So, both features are indicative that Al^{+3} has replaced the Fe^{+3} ions in the crystallographic sites of the unit cell.

When we compare the sample $BaFe_{10.5}Al_{1.5}O_{19}$ (a.k.a. BAL1.5, with the highest aluminum content.) with the undoped sample the cell constants “a” and “c” are reduced by 0.4% and 0.5%, respectively. At the same time, the nanoparticle size of the BAL1.5 sample is slightly greater than that of the undoped sample. This apparent contradiction can be explained by the fact that the crystal of BAL1.5 had started growing from a crystalline cell with a lower and received the same amount of energy to grow as the undoped sample. Therefore it is possible that both samples grew to incorporate the same amount of unit cells.

In addition to determining the nanoparticle size, the Williamson–Hall method [26] allows, from the adjustment of a linear equation, to estimate whether or not there are microstrains in the material’s crystalline lattice and also the value of crystallite size. Fig. 4 shows the adjustments of the Williamson–Hall graphs for each of the precursors used to obtain the mixtures, also Table 2 reports the parameters of cristallite sizes and microtrains determined from those adjustments. In all cases, the value of microstrains is practically zero, which indicates that in the crystal the ions occupy equilibrium positions and their coordination spheres have no deformations.

3.1.2. Magnetic results of the barium ferrite precursors

In Table 3 we present a resume of the magnetic properties values obtained from the M vs. H cycles of the composite samples, acquired at room temperature. The values are the saturation magnetization M_s, the remanent magnetization M_r, the squareness S of the cycles (as the ratio M_r/M_s), the coercivity field H_c and the maximum energy product (B.H) max. The saturation magnetization of each branch was calculated using the “law of approach to saturation” (that is equal to the intersection of the Y axis obtained by linear fits of M *vs.* $1/H^2$ plots at a high magnetic fields). The reported values are the mean value of the resulting values form the ascending and descending branch.

It is clear that the value of coercitivy (H_c) increases when at the same time saturation magnetization (M_s) decreases with the amount of aluminium added to the barium ferrite crystal structure. We interpret

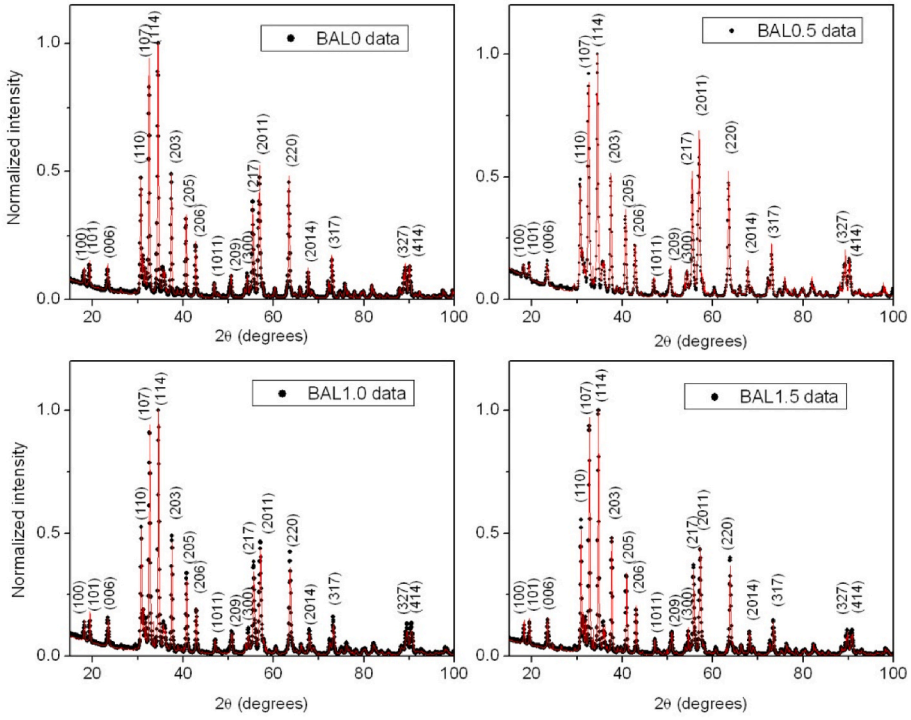

Fig. 1. XRD patterns (dots) of Al-doped barium ferrites with formula $BaFe_{12-x}Al_xO_{19}$ (see nomemclature) with the principal diffraction peaks of barium hexaferrite structure indexed. The solid line is the GSAS-II Rietveld adjusted (normalized) curve.

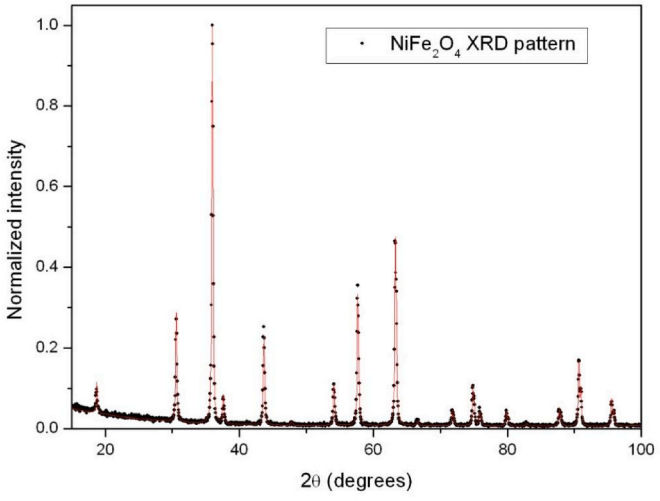

Fig. 2. XRD pattern of the $NiFe_2O_4$ powder (dots) together with fitted curve (solid line).

both phenomena as signals that the Aluminium has been incorporated in to the barium ferrite network.

3.2. *Composite powders (mixtures of Al-doped barium ferrites with nickel ferrite) results*

As mentioned before, for each precursor Al-doped barium ferrite, a composite was created by mixing it with a part of the Nickel Ferrite sample in a percent weight proportion (80% Al-doped ferrite and 20% nickel ferrite). The mixture was ball milled and there after heat-treated as described previously. The following nomenclature applies to the final composites.

Table 2
Cell constants and Rietveld quality refinement parameters of the precursors samples.

Sample	Cell constants (Å)	Crystallite size by Rietveld (nm)	Williamson-Hall size (nm)	Williamson-Hall stress	R_{exp}, R_{wp}, χ^2
BAL0	a = 5.8941_4, c = 23.214_1	17_2	17.6_1	-0.0014_1	4.1, 5.9, 1.7
BAL0.5	a = 5.8742_4, c = 23.135_1	13_3	11.7_1	-0.0012_1	4.3, 8.8, 2.0
BAL1.0	a = 5.8673_4, c = 23.110_1	20_3	22.7_1	-0.0006_1	4.1, 7.8, 1.9
BAL1.5	a = 5.8581_3, c = 23.074_1	22_3	22.1_1	0.0002_1	3.9, 5.0, 1.6
$NiFe_2O_4$	a = 8.3362_5	38_3	35_3	0.0014_1	9.7, 13.1, 1.4

3.2.1. *X-ray diffraction results*

In Fig. 5 we present the X-ray diffraction (XRD) powder patterns of the composite mixtures, together with the curves of Barium Ferrite (BM) phase and the Nickel Ferrite ($NiFe_2O_4$) phase that were part of the total adjusted Rietveld refinement for each sample.

For all composites the XRD profiles also show a moderate broadening of the diffraction peaks, like those XRD patterns corresponding to the precursor ferrites. The presented crystalline phases are Barium Ferrite, Nickel Ferrite, and a small amount of hematite. According to the results of the XRD investigation, the microstructure of the nanostructured composites does not significantly differ from that of their precursor

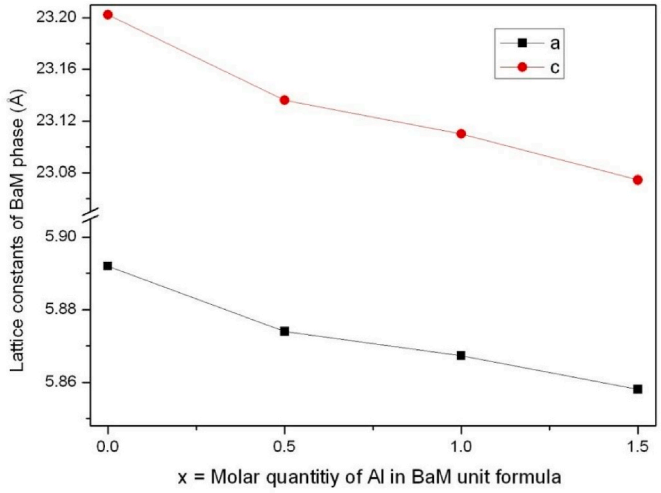

Fig. 3. Unit cell parameters of Al-doped barium ferrites vs. the amount of Al in the chemical unit formula, obtained by Rietveld refinement procedure of the patterns in Fig. 1.

ferrites. This is advantageous for manufacturing the material because, within a specific range, the precursor ferrites' microstructure can be regulated to influence the final product's microstructure. The obtained cell parameters for the principal phases of Barium Ferrite and nickel ferrite are reported in Table 5.

As we mention before, the composites are obtained after a milling process and a thermal treatment to homogenize the defects. The precursor phases of the composites (before the milling) have a nanoparticle size that changes once the process of mechanical mixing and heat treatment has finished.

Comparing the averages nanoparticle size of the phases before and after of being part of the composites (see Tables 2 and 5) we observe that in all cases there is a reduction in it. The reduction in nanoparticle size in hard and soft magnetic phases, only can be explained by means of the effect of mechanical milling, and it is evidence of the transformation of the microstructure of the samples during such process.

In the particular cases that we analyze (composite "M0" and composite "M1.5"), the hexagonal ferrite that forms part of both composites has a practically null value of microtensions (see Williamson-Hall plots in Fig. 6) which indicate that the coordination spheres of metallic ions are in the equilibrium positions and do not possess deformations. The tensions that mechanical milling could have raised were erased by the final thermal treatment.

The nanoparticle size relation between the hard and soft magnetic phases fulfills the condition that the size of the soft phase is not greater than twice the magnetic dominion size of the hard phase; which is suitable to establish exchange coupling magnetic interaction [27]. Nevertheless, as we will describe later, the magnetic measurements show that the mix M0 has minimum coupling interaction, while the mix M1.5 shows such interaction is null. One possible cause of the absence of

Table 3
Magnetic properties of the precursor barium ferrites samples.

Sample	M_s (10^3 A/m)	$S = M_r/M_s$ (no units)	H_c (10^3 A/m)	$(B.H)_{max}$ (10^3 J/m^3)	M_r (10^3 A/m)
BAM0	433.1_2	0.49_1	395_7	10.6_2	211.7_2
BAM0.5	332.2_2	0.49_1	489_9	7.1_2	163.1_2
BAM1.0	318.6_6	0.49_1	561_7	6.7_2	156.8_2
BAM1.5	234.4_4	0.50_1	690_5	3.8_2	116.3_3

Table 4
Composition and nomenclature of the composite samples.

Nomenclature	Sample composition
M0	"BAL0" + $NiFe_2O_4$ (80/20 % wt.)
M0.5	"BAL0.5" + $NiFe_2O_4$ (80/20 % wt.)
M1.0	"BAL1.0" + $NiFe_2O_4$ (80/20 % wt.)
M1.5	"BAL1.5" + $NiFe_2O_4$ (80/20 %wt.)

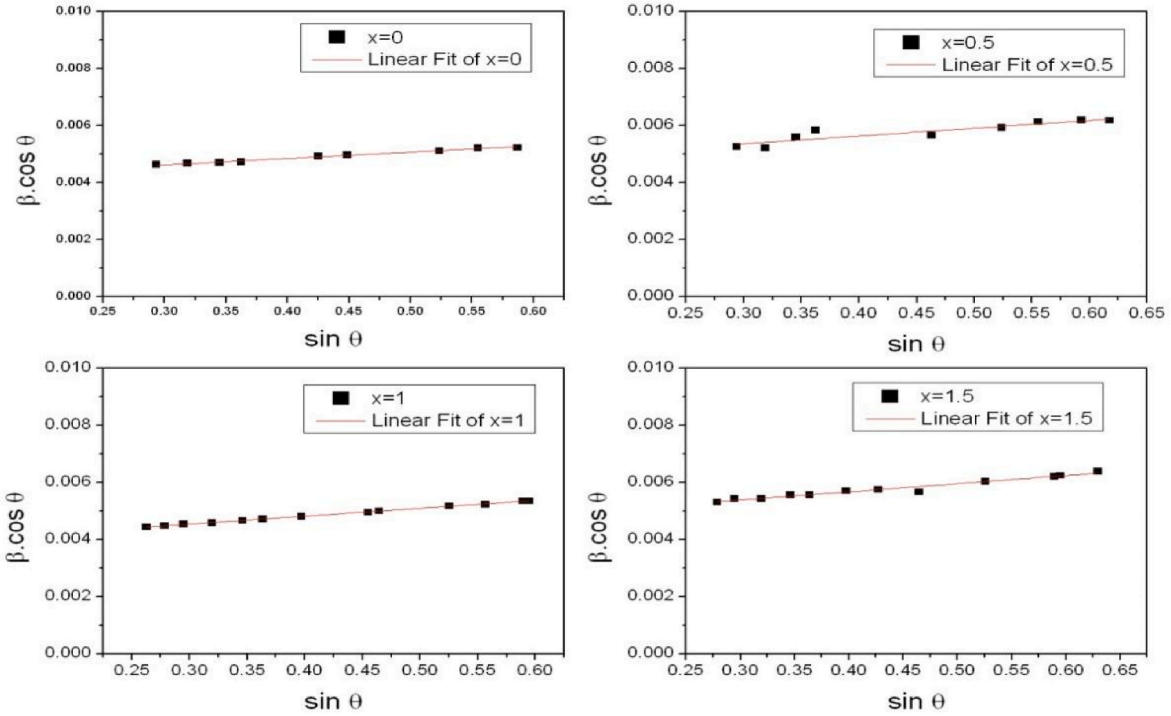

Fig. 4. Williamson-Hall plots of the Al-doped barium ferrite samples.

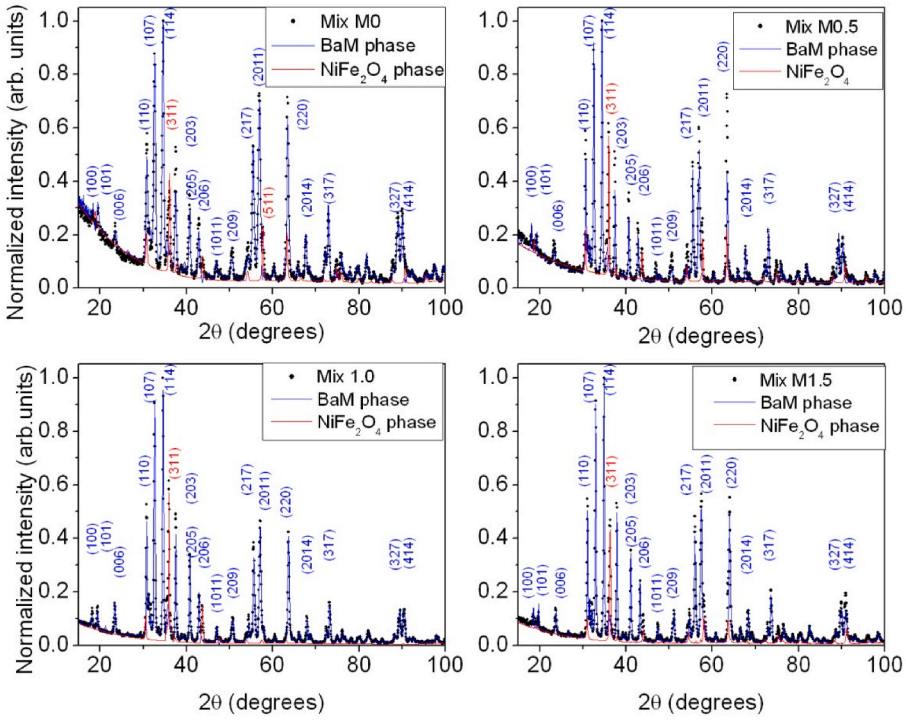

Fig. 5. Experimental XRD patterns (dots) of the composite mixtures (see nomenclature at Table 4), together with the adjusted curves for Barium Ferrite (BaM) phase and nickel ferrite phases (blue and red solid lines respectively). Miller (hkl) indexes of main peaks of barium ferrite (blue) and the principal peak of nickel ferrite (in red) are displayed.

Table 5
Cell constants obtained by Rietveld refinement of the composites.

Sample	BaM cell constants (Å)	BaM Nanoparticle size [nm]	$NiFe_2O_4$ Cell constant (Å)	Rietveld refinement Quality parameters R_{exp}, R_{wp}, χ^2
M0	$a = 5.89128_4$; $c = 23.276_1$	15_1	$a = 8.3426_4$	6.5, 13.4, 2.0
M0.5	$a = 5.8773_4$; $c = 23.150_1$	12_1	$a = 8.32764_5$	5.3, 10.1, 2.0
M1.0	$a = 5.8689_4$; $c = 23.110_1$	19_1	$a = 8.3288_7$	4.1, 7.3, 2.0
M1.5	$a = 5.8459_4$; $c = 23.032_1$	21_1	$a = 8.3130_4$	5.4, 12.5, 2.3

magnetic interaction between the hard and soft magnetic phases, is that the two phases are not in homogeneous contact in the volume of the samples. For a better analysis of this aspect in the next section the microstructure of the mixtures is studied by scanning electron microscopy (SEM).

3.2.2. *Scanning electron microscopy results and magnetic properties of the composites*

In Figs. 7 and 8 we show the SEM micrographics and the EDAX nickel mapping of the samples M0 and M1.5 respectively. It can be observed, in the SEM micrographics, a microstructure with a distribution of conglomerates (clusters) of nanoparticles. The existence of clusters, instead of a uniform distribution of the phases, is the result of the low energy and little spent time in the mechanical milling process. This mentioned conditions of milling, although they were useful to minimize the rise of structural defect and the thermal energy needed to eliminate the microtensions in the crystal network, at the same time were insufficient for accomplishing a homogeneous distribution of the phases.

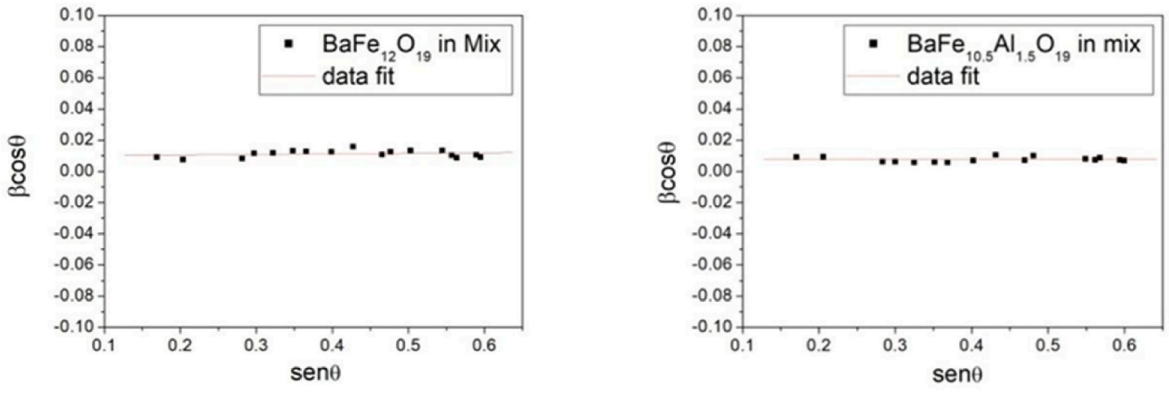

Fig. 6. Williamson-Hall plots of the Barium Ferrite phase in the mix composite sample M0 (left) and in the mix composite sampleM1.5 (right).

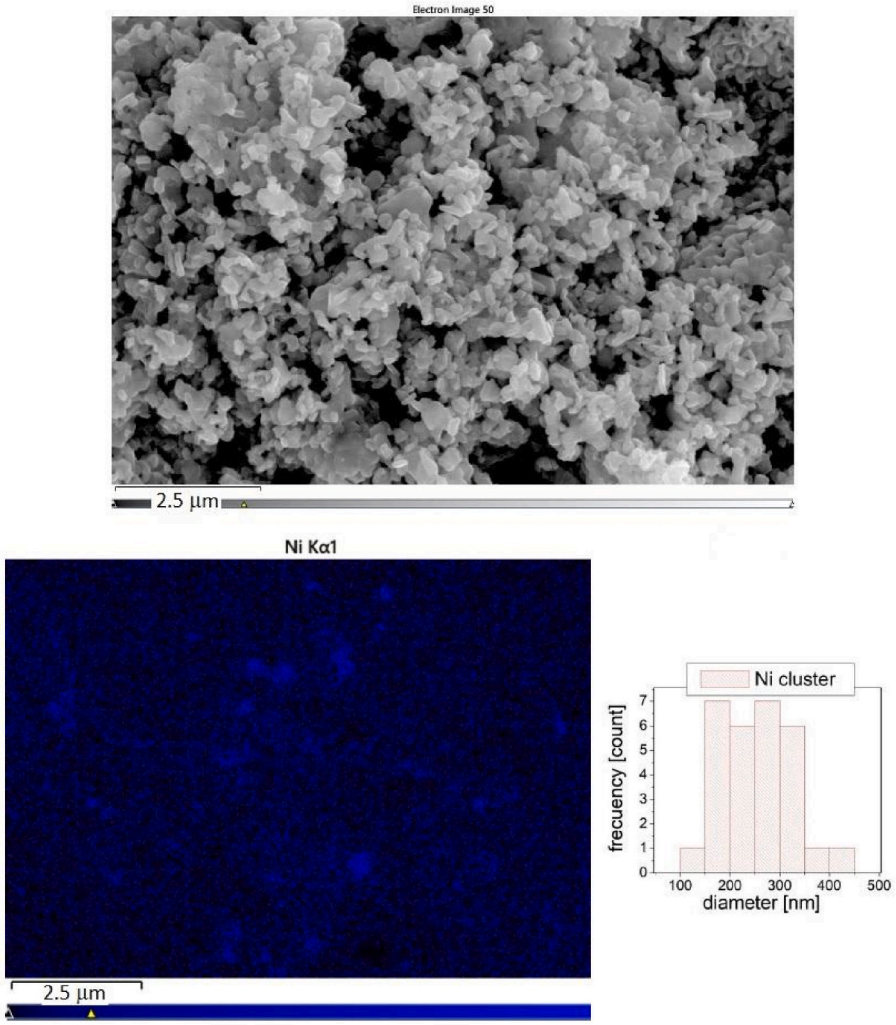

Fig. 7. Scanning electron micrograph of the mix sample (80 wt%) $BaFe_{12}O_{19}$ + (20 wt%) $NiFe_2O_4$ (top) and corresponding nickel EDAX element mapping (bottom left) that allowed us to calculate the size distribution histogram of $NiFe_2O_4$ clusters (bottom right) appearing within the volume of hexagonal ferrite phase.

The grade of homogeneity can be depicted by the spatial distribution of nickel element so to tackle the allocation of the soft magnetic phase of $NiFe_2O_4$ into the volume of the hard magnetic phase of barium ferrite. In the right section of Figs. 7 and 8 the EDAX mapping of Nickel element of the composites M0 and M1.5 is showed to illustrate where the $NiFe_2O_4$ phase appears in the sample, and how it is distributed in that volume. The element mapping of Nickel element shows in both samples, that there are zones with much greater concentration than others. This indicates the lack of homogeneity in the samples. From these element mappings we have constructed histograms (see down right section of Figs. 7 and 8) of the distribution sizes of the agglomerates of $NiFe_2O_4$ in that M0 and M1.5 samples respectively. Since nickel as the element is only present in the composite in the bimetal oxide of $NiFe_2O_4$, the histogram of the nickel cluster size distribution is essentially the same as the nickel ferrite cluster size distribution for each mixture.

The nickel element mapping of the $BaFe_{12}O_{19}/NiFe_2O_4$ (sample M0 undoped BaM mixture), displayed in the down left section of Fig. 7, shows a non-homogeneous distribution with areas of higher concentration than others. These areas correspond to $NiFe_2O_4$ clusters with diameters between 100 nm and 450 nm (see the associated histogram at down right section of Fig. 7). Considering that the average $NiFe_2O_4$ nanoparticles' size is 15 nm in this mixture, it is estimated that the clusters are formed by up to 30 nanoparticles, which are not in contact with the $BaFe_{12}O_{19}$ nanoparticles. This inhomogeneous distribution of magnetically soft phase nanoparticles in the magnetically hard phase volume negatively affects the possibility of exchange coupling interaction.

The inhomogeneity is greater in the mix M1.5 (see micrograph and EDAX mapping in Fig. 8). The histogram of the sizes of the agglomerates of $NiFe_2O_4$ (see the bottom right part of Fig. 8) of this sample shows a wide distribution. In this case the size of the agglomerates reaches to 5 µm which means, taking into the account the size of the nanoparticles (~30 nm), that they are formed by around 160 nanoparticles isolated and therefore not in contact with the hard magnetic phase.

As a result of the described microstructure of the composites and, despite the condition that the nanoparticle size of the soft phase is not greater than twice the size of the magnetic dominion wide of the hard magnetic phase is fulfilled, the exchange coupling interaction is weak. Particularly in the mix M1.5 such interaction is null. This conclusion rises from the analysis of the magnetic measurements. For this we observe Fig. 10 the M vs. H magnetic cycles curves of the M0 and M1.5 samples, and Fig. 11 the Henkel curves of them. Both samples exhibit the presence of the soft magnetic phase, characterized by the shape of their magnetic cycles (wasp-waist-like). The effect is slightly lower in composite M0(Black curve in Fig. 9) compared to composite M1.5 (Green curve in Fig. 9).

Nevertheless, in both cases the shape of the curve is clearly a result of the conjunction of the behaviour of two magnetic phases with mostly dipolar interaction. If the predominant interaction between the phases was the exchange coupling type (instead of dipolar interaction), then

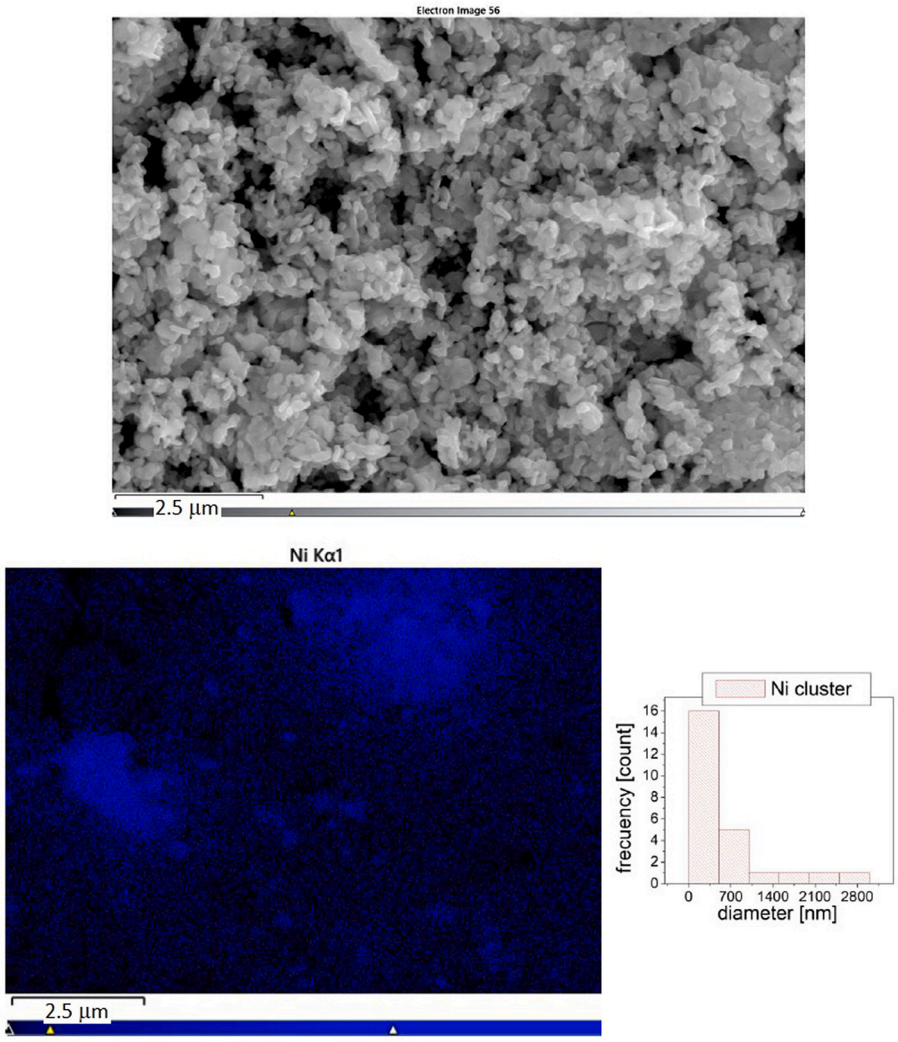

Fig. 8. Scanning electron micrograph of the mix sample (80 wt%) $BaFe_{10.5}Al_{1.5}O_{19}$ + (20 wt%) $NiFe_2O_4$ (top) and corresponding nickel EDAX element mapping (bottom left) that allowed us to calculate the size distribution histogram of $NiFe_2O_4$ clusters (bottom right) appearing within the volume of hexagonal ferrite phase.

then the behaviour (and the shape of the magnetic cycle curve) would be equivalent to a unique single magnetic phase, because when the exchange coupling interaction is dominant the magnetic moments of the atoms of both phases would coherently rotate under the action of the applied magnetic field. We must mention that the obtiananed value of $(B.H)_{max}$ energy product for M0 composite sample was 7.4_2 kJ/m^3, while for M1.5 composite sample was 5.0_1 kJ/m^3. Both mentioned values are lower to the BH product from rare-earth hard magnets, which are in the order of 50–200 kJ/m^3 [19], but again we must recall that we did not achieved exchange-coupling magnetic interaction between the hard and soft magnetic phases.

The Henkel plots (see Fig. 11) give more precise information of the type of magnetic interaction present in the samples [17]. These curves are described by the equation:

$$\delta m = m_d(H) - (1 - 2m_r(H))$$

where δm is the derivative of the Wohlfarth relation ($m_d = 1\text{-}2m_r$) [6], $m_r(H)$ are the values of the isothermal of the remanent magnetization (these values are measured applying an external magnetic field H and then removing it immediately), and m_d are the values of remanent demagnetizing magnetization (it is measured after the maximum remanence has been achieved once the external field H is eliminated).

The interpretation of the Henkel curves is as follows: the maximum with positive slope is associated with a coupling interchange magnetic interaction between the hard and soft magnetic phases. The maximums with negative slope are associated with a dipolar interaction between the phases (demagnetizing interaction).

Considering what was stated in the previous paragraph, we can observe in the detail of the Henkel curve for sample M0 (right section of Fig. 10) there is a small shoulder (the position of it indicated by an arrow) that is a maximum with a positive slope at low fields (between 20 and 40 kA/m). Also in the same plot there is wide maximum at height fields (negative slope). The low intensity of the peak with positive slope can be interpreted as a weak exchange coupling interaction between the hard and soft magnetic phases, while the second maximum at high fields can be interpreted as there is a majority of dipolar interactions between the phases. From intensities peaks relation, we can estimate that there is ~6% of exchange coupling interaction between the phases, so logically 94% rest is dipolar interaction. This is in contrast to the situation described in Ref. [28], where the Henkel plots showed a clear peak indicative of strong exchange coupling, the Henkel plots of our composites showed a peak that was very small compared to the peak corresponding to the dipolar interactions. This suggests that the exchange coupling between the soft and hard magnetic phases in our composites is weak, and that the dipolar interaction is the dominant magnetic interaction.

Now if we observe the Henkel curve corresponding to M1.5 sample

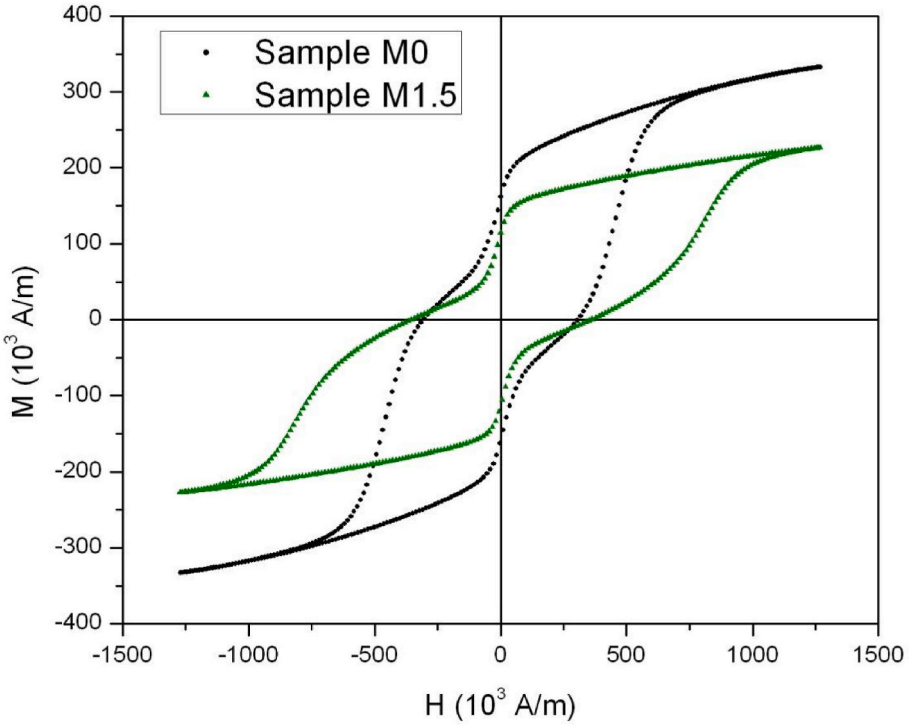

Fig. 9. Magnetization curves of the sample M0 (black dots) and sample M1.5 (green triangles) measured at 300 K.

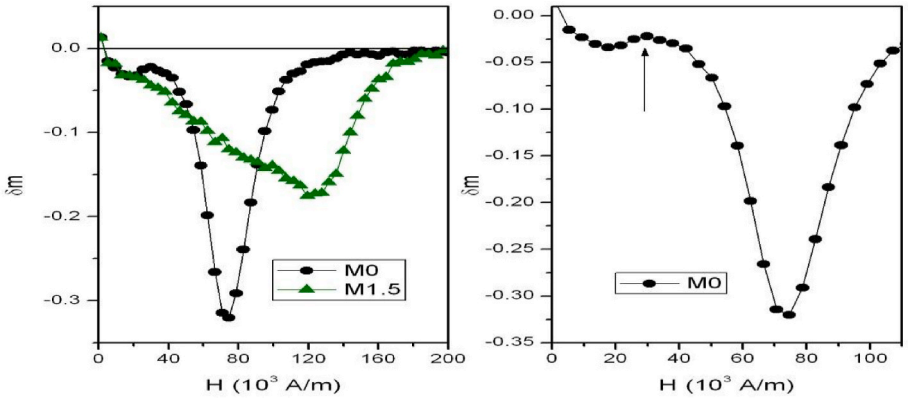

Fig. 10. On the left: Henkel plot of samples M0 (black points) and M1.5 (green triangles). On the right: detail of the Henkel curve for sample M0.

(green dots in the left plot at Fig. 11), the curve has very wide peak (negative slope). This indicates that there are dipolar interactions with total absence of exchange coupling between the hard and soft magnetic phases. The wideness of the peak can be associated with the $NiFe_2O_4$ clustered microstructure presented in this sample that has a broad distribution of cluster sizes, and that they are inhomogeneous scattered in volume of the hexagonal barium ferrite. The biggest clusters have the lower dipolar interaction because there is less contact between phases. The result is what is registered in the Henkel curve, a wide distribution of intensities of the dipolar interaction.

4. Conclusions

We have prepared various hexagonal barium ferrites doped with Aluminium (general formula $BaFe_{12-x}Al_xO_{19}$ with x = 0, 0.05, 0.10 and 0.15) and a sample of nickel ferrites as precursors for composites. The barium ferrites precursors sample showed the contraction of the unit cell parameters, increase of coercivity, and decrease of saturation magnetization as signals of the incorporation of the Aluminium in the barium ferrite network. The composites that we have fabricated are a blend of each barium ferrite (hard magnetic phase) with the nickel ferrite (soft magnetic phase) in an 80/20% weight, mixed by mechanical ball milling and later subjected to thermal treatment to assure the relaxing of the microtensions that might have appear during the milling process. Of the composites manufactured we choose to examine with detail the sample M0 ($BaFe_{12}O_{19}$ with no Al doping + $NiFe_2O_4$ mix) and M1.5 (sample mix $BaFe_{10.5}Al_{1.5}O19$ + $NiFe_2O_4$) for understanding better the relation between microstructure and magnetism. Analysis of those samples in Scanning Electron Microscopy showed that both have large number of wide agglomerates of $NiFe_2O_4$ distributed in the volume of the hexagonal barium ferrite. The inspection of the magnetic cycle and Henkel curves allowed us to correlate the distribution of agglomerates with the magnetic response. We concluded that bigger the clusters, lesser are the chances to establish an exchange correlation magnetic interaction between the hard and the soft magnetic phases even in the case that the relation of nanoparticle sizes are suitable to that interaction. The composites resulted to have a majority or total amount of dipolar magnetic interaction, instead of the wished exchange correlation one, which is

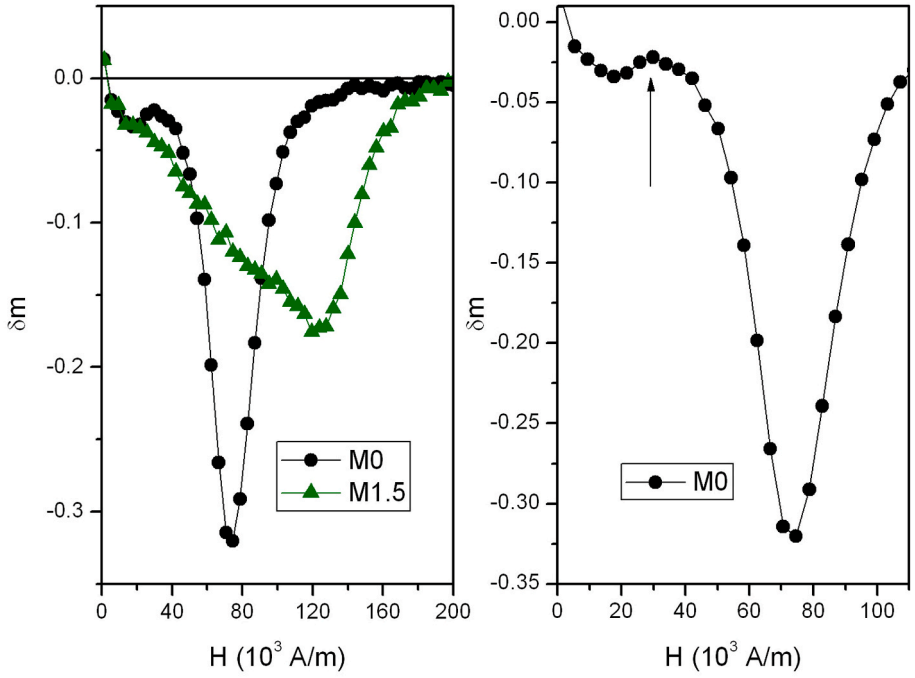

Fig. 11. In the left: Henkel plot of samples M0 (black points) and M1.5 (green triangles). At the right of detail of the Henkel curve for sample M0.

under stable in terms that phases are poorly in contact between them. It is clear that, for achieving that majority of the magnetic interactions can be attributed to the exchange coupling interactions between magnetically hard and soft phases, much more remains to be investigated in the future about the parameters of ball milling (as in Ref. [25]), to settle which parameters are most suited to manufacture a homogeneous mix with no clusters and at the same time disturb with the minimum energy the components of the mix.

Author declaration

We wish to confirm that there are no known conflicts of interest associated with this publication and there has been no significant financial support for this work that could have influenced its outcome.

We confirm that the manuscript has been read and approved by all named authors and that there are no other persons who satisfied the criteria for authorship but are not listed. We further confirm that the order of authors listed in the manuscript has been approved by all of us.

We confirm that we have given due consideration to the protection of intellectual property associated with this work and that there are no impediments to publication, including the timing of publication, with respect to intellectual property. In so doing we confirm that we have followed the regulations of our institutions concerning intellectual property.

We understand that the Corresponding Author is the sole contact for the Editorial process (including Editorial Manager and direct communications with the office). He/she is responsible for communicating with the other authors about progress, submissions of revisions and final approval of proofs. We confirm that we have provided a current, correct email address which is accessible by the Corresponding Author.

Declaration of competing interest

The authors declare that they have no known competing financial interests or personal relationships that could have appeared to influence the work reported in this paper.

Data availability

The data that has been used is confidential.

Acknowledgement

The authors acknowledge the support of CONICET– Argentina and UBACyT 20020190100046BA for funding this research. We thank Dr. V. Bilovol and Dr. K. Berent from AGH University of Krakow for providing the magnetic measurements and SEM facilities.

References

[1] W. Szmaja, SEM investigation of the magnetic domain structure of sintered SmCo5 permanent magnets, Vacuum 83 (Supplement 1) (2009) S249–S251.
[2] D. Derewnicka-Krawczyńska, S. Ferrari, V. Bilovol, M. Pagnola, K. Morawiec, F. D. Saccone, Influence of Nb, Mo, and Ti as doping metals on structure and magnetic response in NdFeB based melt spun ribbons, J. Magn. Magn Mater. (2018) 83–95.
[3] F. Sánchez de Jesús, A.M. Bolarín-Miró, C.A. Cortés-Escobedo, R. Valenzuela, S. Ammar, Mechanosynthesis, crystal structure and magnetic characterization of M-type SrFe12O19, Ceram. Int. 40 (2014) 4033–4038.
[4] A.M. Bolarín-Miró, F. Sánchez de Jesús, C.A. Cortés-Escobedo, S. Díaz de la Torre, R. Valenzuela, Synthesis of M-type SrFe12O19 by mechanosynthesis assisted by spark plasma sintering, Jour. Alloy. Compd 643 (2015) 226–230.
[5] R.A. Nandotaria, R.B. Jotania, C. Singh Sandhu, M. Hashim, S. Singh Meena, P. Bhatt, S.E. Shirsath, Magnetic interactions and dielectric dispersion in Mg substituted M-type Sr-Cu hexaferrite nanoparticles prepared using one step solvent free synthesis technique, Ceram. Int. 44 (Issue 4) (2018) 4426–4435.
[6] J. Singh, C. Singh, D. Kaur, H. Zaki, I.A. Abdel-Latif, S. Bindra Narang, R. Jotania, S.R. Mishra, R.J. oshi, P. Dhruv, M. Ghimire, S.E. Shirsath, S.S. Meena, Elucidation of phase evolution, microstructural, Mössbauer and magnetic properties of $Co^{2+}Al^{3+}$ doped M-type BaSr hexaferrites synthesized by a ceramic method, J. Alloys Comp. 695 (2017) 1112–1121.
[7] S. Shirsath, R.H. Kadam, K.M. Batoo, D. Wang, S. Li1, Co–Al-substituted strontium hexaferrite for rare earth free permanent magnet and microwave absorber application, 2021, J. Phys. D Appl. Phys. 54 (2021), 024001.
[8] E.E. Fullerton, J.S. Jiang, S.D. Bader, Hard/soft magnetic heterostructures: model exchange-spring magnets, J. Magn. Magn Mater. 200 (1–3) (1999) 392–404.
[9] H. Albetran, Y. Slimani, M.A. Almessiere, F. Alahmari, S.E. Shirsath, S. Akhtar, I. M. Low, A. Baykal, I. Ercan, Synthesis, characterization and magnetic investigation of Er-substituted electrospun $NiFe_2O_4$ nanofibers, Phys. Scripta 95 (2020), 075801.
[10] Y. Slimani, M.A. Almessiere, S. Güner, U. Kurtan, S.E. Shirsath, A. Baykal, I. Ercan, Magnetic and microstructural features of Dy^{3+} substituted $NiFe_2O_4$ nanoparticles derived by sol–gel approach, J. Sol. Gel Sci. Technol. 95 (2020) 202–210.

[11] C. Pahwa, S. Mahadevan, S. Bindra Narang, P. Sharma, Structural, magnetic and microwave properties of exchange coupled and non-exchange coupled BaFe12O19/NiFe2O4 nanocomposites, J. Alloys Compd. 725 (2017) 1175–1181.
[12] S.E. Shirsath, C. Cazorla, T. Lu, L. Zhang, Y.Y. Tay, X. Lou, Y. Liu, S. Li, D. Wang, Interface-charge induced giant electrocaloric effect in lead free ferroelectric thin-film bilayers, Nano Lett. 19 (11) (2019) 5006–5013.
[13] S.E. Shirsath, M.H.N. Assadi, J. Zhang, N. Kumar, A.S. Gaikwad, J. Yang, H. E. Maynard-Casely, Y.Y. Tay, J. Du, H. Wang, Y. Yao, Z. Chen, J. Zhang, S. Zhang, S. Li, D. Wang, Interface-driven multiferroicity in cubic BaTiO3-SrTiO3 nanocomposites, ACS Nano 16 (9) (2022) 15413–15424.
[14] Y. Zhao, Co-precipitated Ni/Mn shell coated nano Cu-rich core structure: a phase-field study, J. Mater. Res. Technol. 21 (2) (2022) 546–560.
[15] X. Li, Z.-Q. Dong, L.-P. Wang, X.-D. Niu, H. Yamaguchi, D.-C. Li, P. Yu, A magnetic field coupling fractional step lattice Boltzmann model for the complex interfacial behavior in magnetic multiphase flows, Appl. Math. Model. 106 (2022) 132–152.
[16] Rasband, W.S., ImageJ, U. S. National Institutes of Health, Bethesda, Maryland, USA, https://imagej.nih.gov/ij/, 1997-2018..
[17] J. Garcıa-Otero, M. Porto, J. Rivas, Henkel plots of single-domain ferromagnetic particles, J. Appl. Phys. 87 (2000) 7376–7381.
[18] S.E. Shirsath, D. Wang, S.S. Jadhav, M.L. Mane, S. Li, in: M. Aparicio, A. Jitianu (Eds.), Ferrites Obtained by Sol-Gel Method. (Chapter) Handbook of Sol-Gel Science and Technology, Springer, Cham Klein, L, 2018.
[19] R. Martínez García, V. Bilovol, S. Ferrari, P. de la Presa, P. Marín, M. Pagnola, Structural and magnetic properties of a BaFe12O19/NiFe2O4 nanostructured composite depending on different particle size ratios, J. Magn. Magn. 547 (168934) (2022) 1–12.
[20] C.L. Huang, E. Matijević, Preparation and characterization of ultrafine iron-rich nickel ferrites, Solid State Ionics 84 (3–4) (1996) 249–258.
[21] Y. Shi, J. Ding, X. Liu, J. Wang, NiFe2O4 ultrafine particles prepared by co-precipitation/mechanical alloying, J. Magn. Magn Mater. 205 (2–3) (1999) 249–254.
[22] A.S. Albuquerque, J.D. Ardisson, W.A.A. Macedo, J.L. López, R. Paniago, A.I. C. Persiano, Structure and magnetic properties of nanostructured Ni-ferrite, Jou. Magn. Magn. Mat. 226– 230 (Part 2) (2001) 1379–1381.
[23] B.H. Toby, R.B. Von Dreele, J. Appl. Crystallogr. 46 (2) (2013) 544–549.
[24] X. Obradors, et al., J. Solid State Chem. 56 (1985) 171.
[25] J.M. Hastings, L.M. Corliss, Rev. Mod. Phys. 25 (1953) 114.
[26] G.K. Williamson, W.H. Hall, Acta Metall. 1 (1953) (1953) 22–33.
[27] H. Kronmüller, J. Phys. D Appl. Phys. 29 (1996) 2274.
[28] M.K. Manglam, S. Kumari, J. Mallick, A. Shukla, M. Kar, Magnetic interaction between soft and hard ferrimagnetic phases in $BaFe_{12}O_{19} + CuFe_2O_4$ composite, Phys. Scripta 97 (3) (2022), 035809.